PAPER Special Section on Image Media Quality

Occurrence Prediction of Dislocation Regions in Photoluminescence Image of Multicrystalline Silicon Wafers Using Transfer Learning of Convolutional Neural Network*

Hiroaki KUDO[†a)], **Tetsuya MATSUMOTO**[†], ***Members***, **Kentaro KUTSUKAKE**[††], ***and*** **Noritaka USAMI**[†††], ***Nonmembers***

SUMMARY In this paper, we evaluate a prediction method of regions including dislocation clusters which are crystallographic defects in a photoluminescence (PL) image of multicrystalline silicon wafers. We applied a method of a transfer learning of the convolutional neural network to solve this task. For an input of a sub-region image of a whole PL image, the network outputs the dislocation cluster regions are included in the upper wafer image or not. A network learned using image in lower wafers of the bottom of dislocation clusters as positive examples. We experimented under three conditions as negative examples; image of some depth wafer, randomly selected images, and both images. We examined performances of accuracies and Youden's J statistics under 2 cases; predictions of occurrences of dislocation clusters at 10 upper wafer or 20 upper wafer. Results present that values of accuracies and values of Youden's J are not so high, but they are higher results than ones of bag of features (visual words) method. For our purpose to find occurrences dislocation clusters in upper wafers from the input wafer, we obtained results that randomly select condition as negative examples is appropriate for 10 upper wafers prediction, since its results are better than other negative examples conditions, consistently.

key words: *prediction, transfer learning, convolutional neural network*

1. Introduction

Technologies for manufacturing high-quality silicon wafers for solar cells are being intensively developed, and a novel crystal growth technique has been pursued to permit realization of a high-quality multicrystalline silicon ingot while keeping its advantage of simple directional solidification in a crucible to result in high production yield and low cost. In fact, nucleation control at the bottom of the crucible was recognized as a useful method to control the size of crystal grains in the order of a few *mm*, leading to reduction of the dislocation density. However, dislocation clusters in multicrystalline silicon wafers still remain as one of the main crystal defects to reduce the conversion efficiency of solar cells. For further improvement of the crystal quality of the multicrystalline silicon ingot, we need to somehow suppress the generation of dislocation clusters during crystal growth based on the knowledge of their generating mechanism.

We can observe many grains or 'small regions with different textures' (see Fig. 5) in a multicrystalline silicon wafer. Occurrences of dislocations are affected by crystallographic orientations between neighboring grains, and affect an electrical performance as solar cells. Dislocation clusters in a silicon wafer are invisible with the naked eye, however, we can observe them in a photoluminescence(PL) image which is a particular image.

A PL image records emission lights captured by an infrared camera under an illuminant of a laser light. Dislocations clusters are recorded as dark regions in the image. From this, we can guess dislocations lead a low efficiency as solar cells. We are seeking to clarify to a generating mechanism of dislocation clusters to decrease occurrences of them. At first, we implemented a software that extracts regions of dislocation clusters in a PL image for each sliced wafer in a multicrystalline silicon ingot, and traces regions from bottom to top. We presented the method on visualizing the 3D structures of an evolution of dislocation clusters in a silicon ingot [1] as Fig. 1. The right figure shows the result using wafers from #611 to #868. In a manufacturing process, a multicrystalline silicon ingot is formed by a solidification at the bottom to top in cooling process. In this process, dislocation clusters generate and growth up and shrink.

With this method, we extracted regions of the bottom of dislocation clusters in an silicon ingot to identify a generation point of a dislocation cluster. However, a certain degree of dislocation clusters are required to be recorded as a dark pixel in a PL image. Therefore, a true generation point of a dislocation cluster may exist in lower wafers. We attempted to detect them by more accurate method [2]. We applied detection algorithm to a micro-PL image instead of a (macro-)PL image, and traced dislocation regions. A micro-PL image is a high-resolution image for a smaller area.

However, if we can realize a prediction of candidate areas which includes a true generation point in lower wafer (macro-)PL images, it is useful. We implemented an algorithm based on the image processing to extract dislocation regions in [1]. Next, we introduced a machine learning method to specify them. We tried a matrix decomposition

Manuscript received June 30, 2020.
Manuscript revised October 22, 2020.
Manuscript publicized December 8, 2020.

[†]The authors are with the Graduate School of Informatics, Nagoya University, Nagoya-shi, 464-8601 Japan.
[††]The author is with the Center for Advanced Intelligence Project, RIKEN, Tokyo, 103-0027 Japan.
[†††]The author is with the Graduate School of Engineering, Nagoya University, Nagoya-shi, 464-8603 Japan.

*This paper is an extended version of a manuscript that was presented in the 10th International Workshop on Image Media Quality and its Applications (IMQA2020) [16] with additional descriptions.

a) E-mail: kudo@i.nagoya-u.ac.jp
DOI: 10.1587/transfun.2020IMP0010

Copyright © 2021 The Institute of Electronics, Information and Communication Engineers

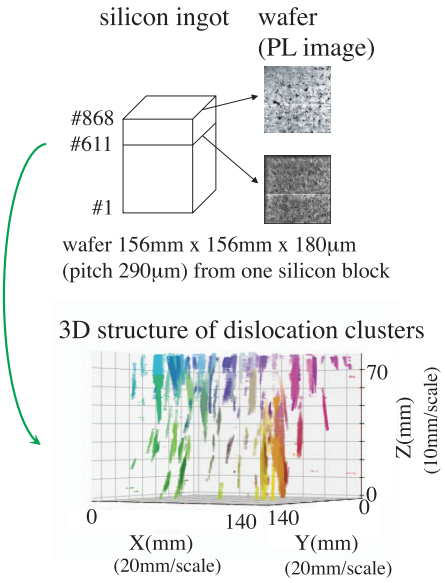

Fig. 1 3D visualization of dislocations clusters.

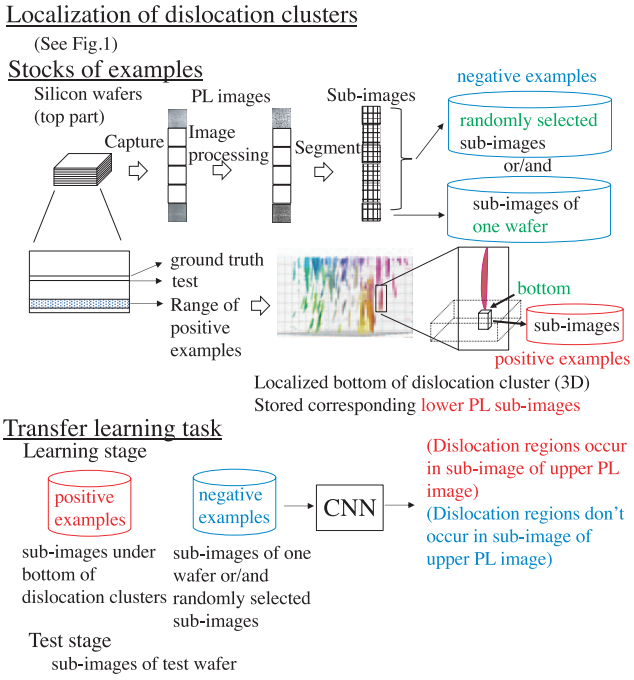

Fig. 2 Outline of proposed method.

method which calculates from a matrix presents pixel intensities of sub-images in a PL image to matrixes express feature images and its coefficients. We applied an algorithm of a dictionary learning framework in a broad sense. Feature images are obtained by independent component analysis and non-negative matrix factorization(NMF) [3] for PL sub-images. NMF is used as a modeling method for a physical phenomenon. For example, it is used as a sound separation algorithm for a power-spectrogram [4], [5], it decomposes a matrix of the spectrogram into an activation matrix and a spectrum matrix. Since an activation matrix is corresponding to a ratio of mixed signals, non-negative is adequate. A spectrum matrix expressed power-spectrum is non-negative, originally. Similarly, parts of an object are separated from an image by an approach of NMF [6], [7]. The values of both mixed ratio and pixel intensities of an image takes non-negative values. As dislocation regions are small part in a wafer, we considered a most of feature images reflect on lots of regions which do not include dislocations. Therefore, regions which include dislocation clusters are extracted according to a criterion that a difference between a reconstruction image calculated by feature images and its coefficients and the original image is large.

Recently, deep neural networks are applied to current practical tasks on a defect detection of solar cells [8], [9]. Defects in these researches are not meant for the same of crystal defects in a silicon wafer as materials in our task, but be a physical damages such as e.g., micro-cracks in the stage of a product testing. The crystal defects of dislocation clusters are not results that occurred by temporal changes in the future as we see in Fig. 1. Before we tried to apply a transfer learning of a convolutional neural network (CNN) to detect the crystal defects, we introduced the multilayer perception (MLP) for the task [10] as a method by a supervised learning. We tried to change the numbers of hidden layers to embed processes of image features extraction and classification. We expected to improve the performance of classification of images, because the network could utilize information of supervised data. However, it performed similar or worse results of NMF as a kind of unsupervised methods. Values of Youden's J described in Sect. 3.2 were obtained about 0.3 for MLP and about 0.3 to 0.7 for NMF. Therefore, we focused on a transfer learning of a convolutional neural network (CNN). As a task of [11], a network classifies an image to a category which includes dislocation regions or a category which does not include dislocation regions from example images of both classes. The network has feed-forward structures, and it learns by supervised-learning method. As a transfer learning, weights of the network is assigned by weights of a pre-trained convolutional neural network (AlexNet [12]). The last layer of its network was replaced by output cells and learned their weights for the task of a dislocation region detection. We experimented and confirmed the performance of this network. We considered a transfer learning framework was appropriate for special uses images or a defect detection task [13], since the number of positive examples are small, relatively. Dislocation clusters regions are only a little in a whole silicon wafer image. Values of Youden's J were obtained similar to values for NMF.

Figure 2 shows the outline of proposed method. In this paper[†], we tried to apply a framework of transfer learning of CNN to predict a generation of dislocation clusters in the upper PL images. In Sect. 2, we explain structures of a network and the prediction task. In Sect. 3, we explain exper-

[†]This paper is an extended version of the manuscript of IMQA2020 [16].

imental conditions, that is, images from some depth wafer, randomly select images, and combined them under the condition with 10 wafers or 20 wafers, and show the results. We examined performances of accuracies and Youden's J statistic [14] changing for negative example settings. We compared results of CNN to the result of a baseline method of bags of features (visual words) [15]. In Sect. 4, we discuss on our results from the view of an occurrence prediction of dislocation clusters. We conjectured that randomly selected negative examples make better results for 10 upper wafers prediction in our task.

2. Method

We used AlexNet [12] as a pre-trained convolutional neural network. As an input to the network, a color image (227×227 pixels, RGB-3 channels) is used. The network outputs one category from 1,000 general image categories.

Figure 3 shows structures of AlexNet. It has 5 convolution layers and 3 fully connected layers. Convolution layer has kernels (or channels, for example, 3 channels in the input layer). A kernel is consisted of 2 dimensional array elements. It works as a filter in image processing. Weights of the network are calculated at the values which were pre-trained by an image classification task of ILSVRC (ImageNet large scale visual recognition challenge).

The 1st, 2nd, and 5th convolution layers process convolution, activation function (Rectified Linear Unit; ReLU), normalization, and max pooling operations. The 3rd and 4th layers process convolution, activation function (ReLU), and normalization operations. The 1st and 2nd fully connected layers process full connection, activation function (ReLU), and dropout operations. The last fully connected layer has full connections, and performs softmax operations to output the one category from 1,000 categories. To see more concretely, the 1st convolution layer operates convolution by filter of size by 11×11 with strides 4×4. It is consisted of 96 kernels. One kernel is composed with a 2-dimensional array by 55×55 elements. After this, max pooling process is done by a filter of size 3×3 with strides 2×2. Finally, 96 kernels which are composed a 2-dimensional array by 27×27 elements were created. The remain convolution layers are perform a similar processes. The 1st and 2nd fully connected layers have weighted connection, and some connections among them were deleted (dropout), randomly. Here, a rate of a dropout was set to 50%.

As a transfer learning, our network kept weights of these connections. These layers work as a feature extractor of an input image. We changed a connection structure of the last full connected layer to classify from 1,000 categories to 2 categories. Two classes correspond to categories whether an input sub-image of a PL image includes dislocation regions in upper wafers or not. Loss function was defined by a calculation of cross-entropies.

In [11], the network outputs one of categories of whether an input image including dislocation clusters or not, for a sub-image of a silicon wafer PL image, directly. To

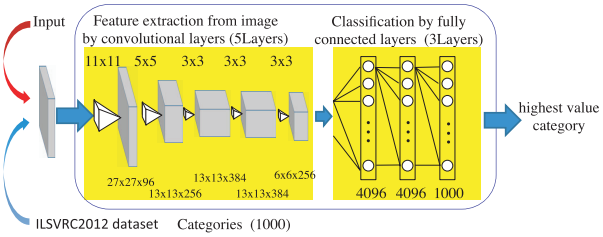

Fig. 3 Structure of AlexNet [16].

compare the task of identification of dislocation clusters region [11], a prediction task in this paper is a hard problem. Example images are collected by identifying a location of the bottom of dislocation clusters and extract further lower 10 or 20 images at the same location in lower wafer. The bottom image of dislocation clusters has very small region as dislocation features. Therefore, lower images are not able to discriminate other conventional region images well. As a technical point, the originated network of transfer learning, that is, AlexNet is trained by a large size which is compared to our input image size, and color image, and natural scenes. On the other hands, the input images (16×16 pixels) are small because we do not identify a silicon wafer which include defects or not, but we identify to locate dislocations regions in a wafer image. And, input images are gray-scale format and 'un-natural scene' or texture images which are far from the training data set. Therefore, we consider that showing results to apply the transfer learning to our tasks is useful for the similar task which uses such special images. In addition, since we show the performance under the conditions with using 10 or 20 wafers as positive examples of learning data, it will have a worth to estimate the numbers or how to select examples for prediction tasks.

We used PL images of sliced wafers from one multicrystalline silicon block. Dimensions of a wafer are 156×156 mm, and thickness is 180 μm. A sliced pitch is 290 μm, we can convert from the number of a wafer to a physical height in a silicon block with this value of the sliced pitch. We assigned an index for each wafer from bottom wafer to top wafer in silicon block. A PL image is a gray-scaled image. We set exposure duration to 2 *sec* under the condition of laser output 80 W (λ=940 nm). In the Fig. 4, we showed a wafer number to use in this paper. The bottom and top wafer is #1 and #868 in a silicon ingot, respectively. The upper part (#611 to #868) in a silicon block which includes lots of dislocation clusters than the lower part is a range of the subject of this paper. Positive examples are extracted from #631 to #680 wafers. Negative examples are extracted from randomly selected from upper part (#611 to #857) or #611 wafer. Input images of a network are segmented images from #751 wafer, regularly. A ground truth is made by identifying regions of the occurrences of dislocation clusters in #761 wafer as the same location of an input image of #751 for a condition using the positive examples of 10 wafers. Similarly, the ground truth of #771 are defined for a condition using the positive examples of 20 wafers.

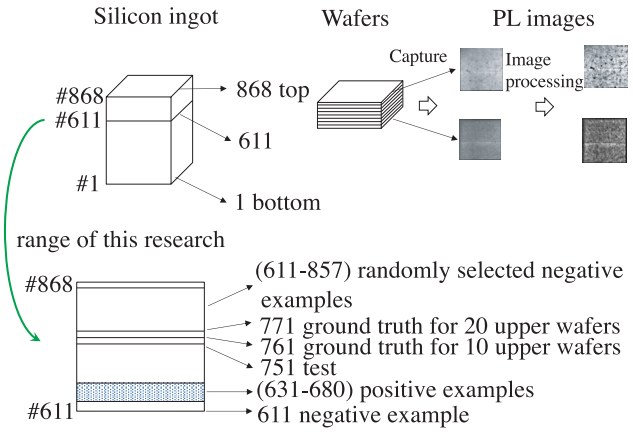

Fig. 4 Wafer properties.

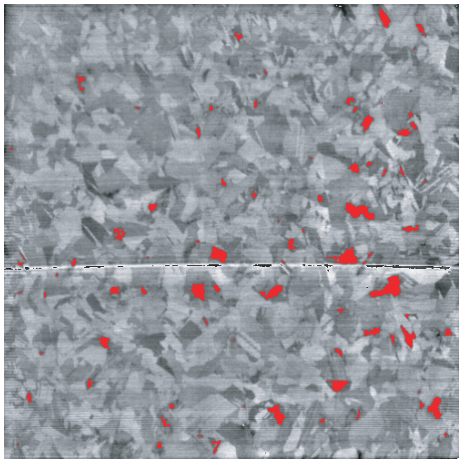

Fig. 5 PL image (#751); red regions present dislocation clusters candidates extracted by image processing [16].

Dislocation clusters whose height has more than 10 wafers are extracted by an image processing procedure are traced and identify the bottom of its clusters. As a possible generation point of dislocation clusters, we stored 10 or 20 images at the same location in lower wafers. To say inversely, the image is a example that it occurs dislocation clusters at the same location within upper 10 or 20 wafers. These are positive examples.

On the other hand, negative examples that are collected by three conditions; 961 images from #611 (the bottom of our treated PL images in this report), 900 images from random selection, and total images of both conditions.

Test images are sampled as sub-image of #751 wafer. Figure 5 shows a PL image of #751 wafer, and red colored regions present extracted regions by image processing as dislocation clusters. This is an enhancement contrasted image after image processing to reduce sliced-marks which are occurred by cutting out wafers from a silicon block [1]. Figure 6 shows examples of (a) images which include dislocation clusters training set, (b) images in #611 wafer, (c) randomly selected images.

Python programs and OpenCV libraries were used to implement these operations on Windows PC.

(a) Lower wafer images of bottom of dislocation clusters (positive examples)

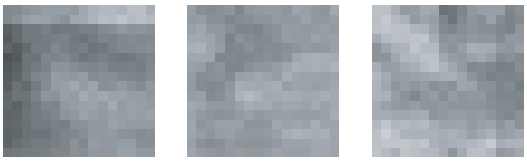

(b) Images of #611 wafer (negative examples)

(c) Random selected images (negative examples)

Fig. 6 Examples of positive and negative examples [16].

3. Experiment

3.1 Input Images and Ground Truth

We segmented an enhanced PL image (500×500 pixels) into sub-regions whose size is 16×16 pixels. A PL image is divided into 31×31 regions as sub-images. 4 pixels regions of right-end and bottom-end were not used. It corresponds to cropping a PL image of a size of 496×496 pixels. AlexNet accepts a color image as an input image. In program, a sub-image of a PL image was converted to a color format image. A ground truth image was defined by a unit of a sub-region (16×16 pixels) by a handwork for image processing results for #751, #761, and #771 wafers. We defined the ground truth as manually, since the identification of regions of the occurrences of dislocation clusters in #761 or #771 which are 10 or 20 upper wafers of a test wafer (#751) is easy to judge whether a segmented area which corresponds to the input image include red-colored pixels by a method [1] in the image like Fig. 5 or not. The number of regions which include dislocations are 152, 165, and 160 for #751, #761, and #771 wafers, respectively. They are not corresponding to the number of dislocation clusters, because that is a common case that one cluster is included in some sub-images.

Image augmented processes of image-shift and flip are performed by inside processes in a program. MATLAB R2018b/R2019b program was used to implement transfer learning on a windows PC (Windows 10 Pro, Intel Core i9-7900X, 32 Gbyte, GPU: NVIDIA Quadro P5000).

3.2 Results

We show results of prediction performances in 10 and 20

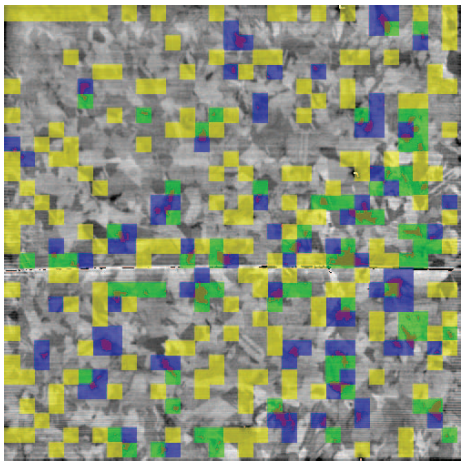

Fig. 7 Example of prediction results on #761 wafer image (10 wafers, 10 epochs, random); green TP, blue FN, yellow FP, no-mark TN.

upper wafers and compared them to results of other method, that is, bag of features (visual words), and examined effects by differences of negative examples. We set mini-batch size at 16. We trained a network in 10, 30, 50, 100 and 200 epochs for training data. Epoch represents the number of displaying turns of all data. 5 trials are performed for each condition. Figure 7 shows an example of prediction results of dislocation regions overlapped on the image of #761 wafer. It shows results of the condition of 10 wafers, 10 epochs, and randomly selected images as negative examples. Green squares correspond to true positive (TP) regions of 78. Blue ones do to false negative (FN) regions of 87. Yellow ones do to false positive (FP) regions of 180. No marked regions do to true negative (TN) regions of 616. In this example, statistics of accuracy and Youden's J are 0.722 and 0.247, respectively.

We calculated accuracies of predictions.

$$Accuracy = \frac{\mathrm{TP} + \mathrm{TN}}{\mathrm{TP} + \mathrm{TN} + \mathrm{FP} + \mathrm{FN}}$$

We also calculated Youden's J statistic [14]. Youden's J is a performance index which is calculated from a sensitivity (TP) /(TP+FN) and a specificity (TN)/(TN+FP). These measures are corresponding to each axis of the ROC (Receiver operating characteristic) curve taking as the value of (1- specificity).

$$\begin{aligned} J &= \text{Sensitivity} - (1 - \text{Specificity}) \\ &= \text{Sensitivity} + \text{Specificity} - 1 \\ &= \frac{\mathrm{TP}}{\mathrm{TP} + \mathrm{FN}} + \frac{\mathrm{TN}}{\mathrm{TN} + \mathrm{FP}} - 1 \end{aligned}$$

3.2.1 20 Wafers Results

Tables 1 and 2 show results in negative examples conditions (611, random, and 611+random) for a prediction for upper 20 wafers when #751 wafer was used as an input. Table 1 shows result of the conditions that correct outputs are defined to correspond to regions including dislocation clusters in #771 wafer which is an upper wafer of an input wafer. On the other hand, Table 2 shows results that correct outputs are defined to regions including dislocation clusters in #771 wafer, however, they do not include dislocation clusters in #751. Because, we thought that the case of dislocation clusters have already occurred was not an interest input, since we expect to predict occurrence of dislocation clusters. In real, it seems probable that dislocation clusters shrink in the upper wafers as Fig. 1. We supposed that dislocation clusters grow up to 10 wafers.

'GT' and 'SD' in columns in each table mean the number of ground truth and sample standard deviation for values of accuracy or Youden's J. The best values show by the colored(red/blue) fonts for each negative example condition for values of accuracy and Youden's J. And, red colored values mean the best in all conditions.

We compared them to results of a prediction based on an algorithm of bag of features (visual words) [15] with the same dataset. We show results in Tables 3 and 4. The best values are shown by red colored fonts.

For a learning stage, accuracies and Youden's J reached at 1 of a theoretical best value at least 50 epochs condition in these trials. For a test stage, values of sample standard deviation of accuracy show smaller according to increase the number of epochs in Tables 1 and 2 for any negative example conditions. Accuracies take values about 0.65 to 0.75 and 0.65 to 0.80, respectively. These values are higher than results about 0.65 of bag of features (visual words) in Tables 3 and 4. Especially, 611+random conditions are better than other negative example conditions. Values of 611+random condition take higher than other conditions. In this experiment, we added example images of both conditions, simply. Therefore, the number of examples are increased, it is reasonable to improve performances. Values in Table 2 reached about 0.8.

However, sensitivities take low scores. Therefore, the higher rate is obtained by improving to increase a correct rate for true negative images. In our purpose, to improve for true positive image is more interest as a meaningful prediction. Therefore, it is thought that Youden J statistics is more important to present for a performance of predictions. Maximum values of Youden's J are obtained from 611+random condition in Table 1 and 611 condition in Table 2. However, scores of Youden's J are low about 0.1. Since Youden's J in results of bag of features are about 0, the results are better than one of bag of features, at least.

To compare between results in Tables 1 and 2, the best value of accuracies is obtained in Table 2 from the view of an occurrence prediction of dislocation clusters. This means a condition excluding images that dislocation clusters has occurred already in an input image is better, although such regions images are not given as examples. The best value of Youden's J degrades low scores in this condition, and 10 epochs result are better than more repeated epochs results.

We couldn't obtain an obvious tendency in Youden's

Table 1 Result of occurrence prediction of 20 upper wafers for #751 wafer input (Dislocation in #771 wafer).

	Condition	Total	GT	TP	FN	FP	TN	Accuracy	SD	Sensitivity	Specificity	J	SD
10	611	961	160	61.0	99.0	224.6	576.4	0.663	0.049	0.381	0.720	0.101	0.033
	random	961	160	65.0	95.0	237.2	563.8	0.654	0.087	0.406	0.704	0.110	0.021
	611+random	961	160	44.6	115.4	131.6	669.4	0.743	0.041	0.279	0.836	0.114	0.010
30	611	961	160	45.0	115.0	167.4	633.6	0.706	0.032	0.281	0.791	0.072	0.042
	random	961	160	54.8	105.2	210.4	590.6	0.672	0.039	0.343	0.737	0.080	0.033
	611+random	961	160	31.6	128.4	96.8	704.2	0.766	0.008	0.198	0.879	0.077	0.025
50	611	961	160	58.8	101.2	204.2	596.8	0.682	0.035	0.368	0.745	0.113	0.026
	random	961	160	55.6	104.4	193.8	607.2	0.690	0.020	0.348	0.758	0.106	0.022
	611+random	961	160	30.0	130.0	93.6	707.4	0.767	0.004	0.188	0.883	0.071	0.018
100	611	961	160	52.4	107.6	197.8	603.2	0.682	0.021	0.328	0.753	0.081	0.026
	random	961	160	55.2	104.8	192.6	608.4	0.691	0.010	0.345	0.760	0.105	0.040
	611+random	961	160	32.0	128.0	98.6	702.4	0.764	0.009	0.200	0.877	0.077	0.010
200	611	961	160	58.2	101.8	216.8	584.2	0.668	0.008	0.364	0.729	0.093	0.016
	random	961	160	51.6	108.4	195.2	605.8	0.684	0.009	0.323	0.756	0.079	0.022
	611+random	961	160	29.4	130.6	95.2	705.8	0.765	0.007	0.184	0.881	0.065	0.028

Table 2 Result of occurrence prediction of 20 upper wafers for #751 wafer input (Dislocation in #771 wafer, not dislocation in #751).

	Condition	Total	GT	TP	FN	FP	TN	Accuracy	SD	Sensitivity	Specificity	J	SD
10	611	961	85	32.0	53.0	253.6	622.4	0.681	0.058	0.376	0.711	0.087	0.021
	random	961	85	30.2	54.8	272.0	604.0	0.660	0.112	0.355	0.689	0.045	0.030
	611+random	961	85	20.6	64.4	155.6	720.4	0.771	0.053	0.242	0.822	0.065	0.038
30	611	961	85	22.2	62.8	190.2	685.8	0.737	0.051	0.261	0.783	0.044	0.013
	random	961	85	24.0	61.0	241.2	634.8	0.686	0.044	0.282	0.725	0.007	0.033
	611+random	961	85	12.4	72.6	116.0	760.0	0.804	0.011	0.146	0.868	0.013	0.023
50	611	961	85	30.0	55.0	233.0	643.0	0.700	0.040	0.353	0.734	0.087	0.029
	random	961	85	25.4	59.6	224.0	652.0	0.705	0.030	0.299	0.744	0.043	0.020
	611+random	961	85	13.0	72.0	110.6	765.4	0.810	0.010	0.153	0.874	0.027	0.033
100	611	961	85	26.0	59.0	224.2	651.8	0.705	0.024	0.306	0.744	0.050	0.028
	random	961	85	24.2	60.8	223.6	652.4	0.704	0.009	0.285	0.745	0.029	0.028
	611+random	961	85	12.8	72.2	117.8	758.2	0.802	0.010	0.151	0.866	0.016	0.018
200	611	961	85	29.0	56.0	246.0	630.0	0.686	0.013	0.341	0.719	0.060	0.039
	random	961	85	22.8	62.2	224.0	652.0	0.702	0.012	0.268	0.744	0.013	0.041
	611+random	961	85	11.8	73.2	112.8	763.2	0.806	0.006	0.139	0.871	0.010	0.012

Table 3 Result of occurrence prediction of 20 upper wafers for #751 wafer input (Dislocation in #771 wafer) (Bag of features).

	Condition	Total	GT	TP	FN	FP	TN	Accuracy	SD	Sensitivity	Specificity	J	SD
BOF	611	961	160	53.8	106.2	253.6	547.4	0.626	0.009	0.336	0.683	0.020	0.036
	random	961	160	51.6	108.4	244.2	556.8	0.633	0.019	0.323	0.695	0.018	0.044
	611+random	961	160	50.4	109.6	233.4	567.6	0.643	0.007	0.315	0.709	0.024	0.025

Table 4 Result of occurrence prediction of 20 upper wafers for #751 wafer input (Dislocation in #771 wafer, not dislocation in #751) (Bag of features).

	Condition	Total	GT	TP	FN	FP	TN	Accuracy	SD	Sensitivity	Specificity	J	SD
BOF	611	961	85	27.8	57.2	279.6	596.4	0.650	0.008	0.327	0.681	0.008	0.043
	random	961	85	26.0	59.0	269.8	606.2	0.658	0.018	0.306	0.692	-0.002	0.047
	611+random	961	85	24.4	60.6	259.4	616.6	0.667	0.010	0.287	0.704	-0.009	0.031

J for changing negative example conditions. For example. the best values for the same epochs in Table 1 are obtained in various conditions, that is, 611+random condition for 10 epochs, random conditions for 30 epochs, and 611 conditions for 50 epochs. The positive examples are same for these settings. It implies that differences among negative examples conditions did not work effectively for predictions, that is, it may mean a way of 20 wafers sampling is too much for correcting examples.

3.2.2 10 Wafers Results

Tables 5 and 6 show results of a prediction for 10 upper wafers when #751 wafer was used as an input. Table 5 corresponds to occurrence predictions of dislocation clusters in #761 wafer for #751 wafer as an input. Table 6 shows results for dislocation clusters in #761, but it's not dislocation clusters in #751. We compared them to results of bag of

Table 5 Result of occurrence prediction of 10 upper wafers for #751 wafer input (Dislocation in #761 wafer).

	Condition	Total	GT	TP	FN	FP	TN	Accuracy	SD	Sensitivity	Specificity	J	SD
10	611	961	165	41.0	124.0	85.4	710.6	0.782	0.020	0.248	0.893	0.141	0.012
	random	961	165	56.6	108.4	111.0	685.0	0.772	0.029	0.343	0.861	0.204	0.029
	611+random	961	165	33.0	132.0	50.2	745.8	0.810	0.010	0.200	0.937	0.137	0.026
30	611	961	165	40.0	125.0	91.6	704.4	0.775	0.024	0.242	0.885	0.127	0.017
	random	961	165	48.0	117.0	102.4	693.6	0.772	0.007	0.291	0.871	0.162	0.051
	611+random	961	165	31.6	133.4	55.2	740.8	0.804	0.009	0.192	0.931	0.122	0.014
50	611	961	165	40.4	124.6	93.4	702.6	0.773	0.018	0.245	0.883	0.128	0.033
	random	961	165	54.2	110.8	111.0	685.0	0.769	0.015	0.328	0.861	0.189	0.024
	611+random	961	165	29.4	135.6	54.6	741.4	0.802	0.008	0.178	0.931	0.110	0.011
100	611	961	165	37.0	128.0	87.2	708.8	0.776	0.003	0.224	0.890	0.115	0.008
	random	961	165	51.8	113.2	95.4	700.6	0.783	0.009	0.314	0.880	0.194	0.041
	611+random	961	165	28.8	136.2	45.4	750.6	0.811	0.003	0.175	0.943	0.118	0.016
200	611	961	165	37.2	127.8	89.8	706.2	0.774	0.012	0.225	0.887	0.113	0.006
	random	961	165	53.8	111.2	108.2	687.8	0.772	0.004	0.326	0.864	0.190	0.018
	611+random	961	165	26.6	138.4	45.6	750.4	0.809	0.005	0.161	0.943	0.104	0.018

Table 6 Result of occurrence prediction of 10 upper wafers for #751 wafer input (Dislocation in #761 wafer, not dislocation in #751).

	Condition	Total	GT	TP	FN	FP	TN	Accuracy	SD	Sensitivity	Specificity	J	SD
10	611	961	54	11.6	42.4	114.8	792.2	0.836	0.028	0.215	0.873	0.088	0.043
	random	961	54	14.8	39.2	152.8	754.2	0.800	0.044	0.274	0.832	0.106	0.056
	611+random	961	54	7.0	47.0	76.2	830.8	0.872	0.013	0.130	0.916	0.046	0.033
30	611	961	54	12.0	42.0	119.6	787.4	0.832	0.030	0.222	0.868	0.090	0.022
	random	961	54	11.6	42.4	138.8	768.2	0.811	0.023	0.215	0.847	0.062	0.039
	611+random	961	54	7.2	46.8	79.6	827.4	0.868	0.009	0.133	0.912	0.046	0.026
50	611	961	54	11.6	42.4	122.2	784.8	0.829	0.026	0.215	0.865	0.080	0.037
	random	961	54	14.2	39.8	151.0	756.0	0.801	0.018	0.263	0.834	0.096	0.024
	611+random	961	54	5.6	48.4	78.4	828.6	0.868	0.009	0.104	0.914	0.017	0.027
100	611	961	54	10.0	44.0	114.2	792.8	0.835	0.006	0.185	0.874	0.059	0.026
	random	961	54	12.6	41.4	134.6	772.4	0.817	0.025	0.233	0.852	0.085	0.024
	611+random	961	54	6.8	47.2	67.4	839.6	0.881	0.004	0.126	0.926	0.052	0.031
200	611	961	54	11.0	43.0	116.0	791.0	0.835	0.017	0.204	0.872	0.076	0.039
	random	961	54	14.6	39.4	147.4	759.6	0.806	0.009	0.270	0.837	0.108	0.030
	611+random	961	54	5.8	48.2	66.4	840.6	0.881	0.007	0.107	0.927	0.034	0.012

Table 7 Result of occurrence prediction of 10 upper wafers for #751 wafer input (Dislocation in #761 wafer) (Bag of features).

	Condition	Total	GT	TP	FN	FP	TN	Accuracy	SD	Sensitivity	Specificity	J	SD
BOF	611	961	165	42.8	122.2	205.0	591.0	0.660	0.005	0.259	0.742	0.002	0.032
	random	961	165	44.6	120.4	221.2	574.8	0.645	0.007	0.270	0.722	-0.008	0.035
	611+random	961	165	44.4	120.6	207.0	589.0	0.659	0.013	0.269	0.740	0.009	0.020

Table 8 Result of occurrence prediction of 10 upper wafers for #751 wafer input (Dislocation in #761 wafer, not dislocation in #751) (Bag of features).

	Condition	Total	GT	TP	FN	FP	TN	Accuracy	SD	Sensitivity	Specificity	J	SD
BOF	611	961	54	11.0	43.0	236.8	670.2	0.709	0.011	0.204	0.739	-0.057	0.042
	random	961	54	11.6	42.4	254.2	652.8	0.691	0.007	0.215	0.720	-0.065	0.078
	611+random	961	54	13.4	40.6	238.0	669.0	0.710	0.015	0.248	0.738	-0.014	0.037

features (visual words) are shown in Tables 7 and 8.

The best values of accuracies are obtained by the 611+random condition. The values are higher than 20 upper wafers predictions. Results of bag of features are also improved about 0.02 (Table 7) and 0.05 (Table 8). However, amounts of improvement in results of transfer leaning are larger than them, that is, about 0.04 (Table 5) and 0.07 (Table 6). The sensitivities are low under the conditions that accuracies are high as similar to results of 20 wafers case.

We focused on values of Youden's J. Maximum values of Youden's J were obtained under the condition of randomly selected negative examples. In any epochs conditions, it can be seen a similar tendency, although 20 wafers results are not clear for differences of conditions of negative examples. These values are higher than results of 20 upper wafers prediction. Amounts of improvement scores are about 0.1 points from values in Table 1 and 0.02 from ones in Table 2. Since results of bag of features are about 0, and

it is worse than results of 20 wafers case. results of transfer learning are better than ones of bag of features.

To compare results in Tables 5 and 6, the best result of J in Table 6 that is the condition of dislocation regions images are exclude is lower than the best value in Table 5. In 10 wafers condition, it shows a tendency that values of J under the condition using randomly selected images as negative examples are larger, as epochs are increased. Therefore, we consider that 10 wafers sampling for a randomly selected way as a negative examples fit for this prediction task. To compare between 611 and 611+ random, we can see that random examples takes a role of increasing both the sensitivity and a specificity. To compare between random and 611+ random, we can see that 611 examples takes a role of decreasing the sensitivity and increasing a specificity. Since 611+ conditions leads increasing the total numbers of negative examples, it is a reasonable specificity is increase. However, 611 examples lead to underperformance.

4. Discussion

We applied transfer learning to occurrence predictions of dislocation clusters in 10 or 20 upper wafers. Both indexes of accuracies and Youden's J did not reach at 1 for test images (sub-images of #751 wafer). Accuracies are 0.7 to 0.8, and Youden's Js are 0.1 to 0.2, approximately, they are low scores. Predictions in 20 upper wafers are worse results than ones in 10 upper wafers. The results in 20 wafers, obvious tendencies are not obtained for differences of negative examples conditions. We conjecture that 20 upper wafers prediction is more difficult task than predictions in 10 upper wafers under this experiment settings. It may mean that 20 wafer sampling is too much for predictions. It may include some of them are not appreciate examples as positive examples. It is difficult for even 10 upper wafers prediction condition, when we evaluate the performances by the values of Youden's J. However, we obtained a tendency in the condition of using randomly selected image as negative examples. Based on the this, we obtained the guide of selections of the negative examples. A randomly selection way is better than an extraction way from one specific wafer. It may show the some image features for each layer have an inherent property even we can't see image features by an appearance of an sub-image. It is an interesting point from the view of the physical grains structures composed in a sub-image, if it is embedded the information of a crystalline growth mechanism. Humans can't see it through image features, the network can utilize the image features.

As a reason that we examine the results under a condition that a sub-image includes dislocation clusters in a prediction wafer and does not include dislocation clusters at the same location in input wafer (Tables 2 and 6), we desire to predict to occur a new generation point of dislocation clusters. Therefore, we expected to exclude the same dislocation clusters by an above criterion. However, this criterion allows to include detections of regions which are caused by a growth up of neighbor dislocation clusters in the input wafer. Dislocation clusters do not always extend upwards. Slant clusters are often observed. Some values of results in Tables 2 and 6 will include predictions of this case.

5. Conclusion

We examined a prediction method of occurrences of dislocation clusters in the upper wafers. We applied a method of a transfer learning of the convolutional neural network to realize a prediction system. As positive examples, images are collected the lower 20 wafers or 10 wafers from the bottom of dislocation clusters. Performances of predictions were examined under three conditions of negative examples, images of some depth wafer (#611), or randomly selected images, or both images. We showed results of accuracies and Youden's J statistic. Performances were not so high, however, these are higher than results by a method of bag of features (visual words). Indexes from sensitivity and specificity show low values, however, we obtained results that randomly select condition as negative examples is better in 10 upper wafers prediction. For 20 upper wafers prediction, the differences of negative examples are not seen as an obvious tendency. It implies that 20 wafers sampling is over to perform the prediction task, and it includes unappreciate examples as positive examples. From different negative samplings, A randomly selection way is better than an extraction way from one specific wafer. Although sampling of one specific wafer leads the underperformance of the network, the system can utilized the image features for each layer have an inherent property even we can't see image features by an appearance of an sub-image.

For further improvement, we are planning to introduce not only pixel intensities of sub-image of a wafer but physical properties of a wafer as input of neural networks.

Acknowledgments

This research was supported in part by JST/CREST (JPMJCR17J1).

References

[1] Y. Hayama, T. Matsumoto, T. Muramatsu,, K. Kutsukake, H. Kudo, and N. Usami, "3D visualization and analysis of dislocation clusters in multicrystalline silicon ingot by approach of data science," Solar Energy Materials and Solar Cells, vol.189, pp.239–244, 2019.
[2] K. Tajima, K. Kutsukake, T. Matsumoto, H. Kudo, and N. Usami, "The relationship between detection of dislocation clusters in multicrystalline silicon through image processing of macro PL images and carrier recombination," 79th JSAP Autumn Meeting, 20a-133-2, 2018 (in Japanese).
[3] H. Kudo, Y. Hayama, T. Matsumoto, K. Kutsukake, and N. Usami, "Estimation by non-matrix factorization of dislocation regions in photoluminescence image of multicrystalline silicon," IEICE Technical Report, 117, 356, pp.13–18, 2017 (in Japanese).
[4] M.N. Schmidt and M. Mørup,"Nonnegative matrix factor 2-D deconvolution for blind single channel source separation," Proc. 6th international conference on Independent Component Analysis and Blind Signal Separation (ICA'06), pp.700–707, 2006.
[5] M.N. Schmidt and R.K. Olsson, "Single-channel speech separation

using sparse non-negative matrix factorization," INTERSPEECH-2006 ICSLP, 2614–2617, 2006.
[6] D.D. Lee and H.S. Seung,"Learning the parts of objects by non-negative matrix factorization," Nature, vol.401, pp.788–791, 1999.
[7] W. Liu and N. Zheng, "Non-negative matrix factorization based methods for object recognition," Pattern Recognition Letters, vol.25, no.8, pp.893–897, 2004.
[8] W. Tang, Q. Yang, K. Xiong, and W. Yan, "Deep learning based automatic defect identification of photovoltaic module using electroluminescence images," Solar Energy, vol.201, pp.453–460, 2020.
[9] M.W. Akram, G. Li, Y. Jin, X. Chen, C. Zhu, X. Zhao. A. Khaliq, M. Faheem, and A. Ahmad, "CNN based automatic detection of photovoltaic cell defects in electroluminescence images," Energy, vol.189, 116319, 2019.
[10] H. Kudo, T. Matsumoto, K. Kutsukake, and N. Usami, "Examination of dimensionality of multilayer perceptron estimating dislocation regions in multicrystalline silicon photoluminescence image," IEICE Technical Report, 118, 256, pp.19–24, 2018 (in Japanese).
[11] H. Kudo, Y. Hayama, T. Matsumoto, K. Kutsukake, and N. Usami, "Prediction of regions including dislocations in multicrystalline silicon photoluminescence image by transfer learning of convolutional neural network," ICONIP 2019 Proceedings (Australian Journal of Intelligent Information Processing Systems), vol.15, no.2, pp.68–74, 2019.
[12] A. Krizhevsky, I. Sutskever, and G.E. Hinton, "ImageNet classification with deep convolutional neural networks," Advances in Neural Information Processing Systems, vol.25, pp.1097–1105, 2012.
[13] M.W. Akram, G. Li, Y. Jin, X. Chen, C. Zhu, and A. Ahmad, "Automatic detection of photovoltaic module defects in infrared images with isolated and develop-model transfer deep learning," Solar Energy, vol.198, pp.175–186, 2020.
[14] W.J. Youden, "Index for rating diagnostic tests," Cancer, vol.3, no.1, pp.32–35, 1950.
[15] G. Csurka, C.R. Dance, L. Fan, J. Willamowski, and C. Bray, "Visual categorization with bags of keypoints," Workshop on Statistical Learning in Computer Vision, ECCV, 1, 2004.
[16] H. Kudo, T. Matsumoto, K. Kutsukake, and N. Usami, "Occurrence prediction of dislocation regions in photoluminescence image of multicrystalline silicon wafers using transfer learning of convolutional neural network," Proc. 10th International Workshop on Image Media Quality and its Applications (IMQA2020), OS3-2-1–OS3-2-5, 2020.

Hiroaki Kudo received the degrees of B. Eng., M. Eng. and D. Eng. at Nagoya University, Japan in 1991, 1993 and 1996, respectively. In April 1996, he was a faculty member of Nagoya University as a Research Associate. In April 1999, he was an Assistant Professor. Since August 2000, he has been an Associate Professor. Currently, he is a member of Graduate School of Informatics, Nagoya University. He was a Research Fellow of the Japan Society for the Promotion of Science in 1995. His research interests include visual perception and computer vision.

Tetsuya Matsumoto received the degrees of B. Eng., M. Eng. and Dr. Eng. from Nagoya University, Nagoya, Japan, in 1982, 1984 and 1996, respectively. From 1984 to 1989, he worked in Toshiba Corporation, Fuchu, Japan. In 1993, he joined Education Center for Information Processing, Nagoya University. In 1998, He moved to Department of Information Engineering, Graduate School of Engineering, Nagoya University. His current interests include neural networks, image processing and machine learning. He is a member of JNNS of Japan and JSAI of Japan.

Kentaro Kutsukake is Postdoctoral Researcher of Center for Advanced Intelligence Project, RIKEN. He received the degrees of B. Sci., M. Sci. and Dr. Sci from Tohoku University in 2002, 2004 and 2007, respectively. From April 2007 to July 2007, he worked as a research fellowship for young scientists (PD) in Japan Society for the Promotion of Science. From August 2007 to March 2010 and from August 2010 to October 2017, he worked as an assistant professor at Institute for Materials Research, Tohoku University. From April 2010 to July 2010, he worked as an assistant professor at Graduate School of Energy Science, Kyoto University. From November 2017 to July 2018, he worked as a designated lecturer at Institutes of Innovation for Future Society. Since August 2018, he has been with RIKEN. His current research interest is application of data science technique to the research of crystal engineering.

Noritaka Usami is Professor of Graduate School of Engineering at Nagoya University. He received the B.E. and M.E. degrees from the University of Tokyo in 1991 and 1993, respectively. From July 1994 to January 2000, he worked as a research associate at Research Center for Advanced Science and Technology, The University of Tokyo. After recieving his phD in January 1998, he spent 10 months at Institüt für Angewandte Photophysik, Technische Universität Dresden as a visiting researcher. From February 2000 to March 2013, he worked as an associate professor at Institute for Materials Research, Tohoku University. Since 2013, he has been with Nagoya University. His research interest covers crystal growth and characterizations of Si-based materials for photovoltaic and electronic applications, and development of a new methodology for novel materials by fusion of experiments, computation, and data science. He has received various awards, including the best paper award at PVSEC (2009), the best poster award at IEEE PVSC (2012), JSPS Innovative PV Award (2017), and so on.